

Abstract—Magnetic resonance imaging (MRI) super-resolution (SR) methods that computationally enhance low-resolution acquisitions to approximate high-resolution quality offer a compelling alternative to expensive high-field scanners. In this work we investigate an elucidated diffusion model (EDM) framework for brain MRI SR and compare two U-Net backbone architectures: (i) a full 3D convolutional U-Net that processes volumetric patches with 3D convolutions and multi-head self-attention, and (ii) a 2.5D slice-conditioned U-Net that super-resolves each slice independently while conditioning on an adjacent slice for inter-slice context. Both models employ continuous-sigma noise conditioning following Karras et al. and are trained on the NKI cohort of the FOMO60K dataset. On a held-out test set of 5 subjects (6 volumes, 993 slices), the 3D model achieves 37.75 dB PSNR, 0.997 SSIM, and 0.020 LPIPS, improving on the off-the-shelf pretrained EDSR baseline (35.57 dB / 0.024 LPIPS) and the 2.5D variant (35.82 dB) across all three metrics under the same test data and degradation pipeline.

Index Terms—Brain MRI, convolutional neural network, denoising diffusion model, elucidated diffusion model, image super-resolution, 3D U-Net.

Comparative Analysis of 3D Convolutional and 2.5D Slice-Conditioned U-Net Architectures for MRI Super-Resolution via Elucidated Diffusion Models

Hendrik Chiche, Ludovic Corcos, and Logan Rouge

Preprint notice: This is a preprint of a paper submitted to *IEEE Access* and currently under peer review. The content is identical to the submitted manuscript. This preprint is made available under IEEE’s author-posting policy.

Source code: <https://github.com/Magic-Solutions/MRI-Super-Resolution>
 Pretrained weights: <https://huggingface.co/Chichonnade/Comparative-Analysis-3D-2.5D-MRI-Super-Resolution-EDM>

I. INTRODUCTION

Clinical MRI scanners operating at 1.5T remain the most widely installed systems worldwide. Although 3T and 7T scanners deliver higher signal-to-noise ratio and finer spatial resolution, their substantially higher procurement and maintenance costs restrict availability, particularly in low-resource settings [11]. Computational super-resolution provides a software-based pathway to bridge this gap.

Traditional interpolation techniques—bicubic, trilinear—produce overly smooth outputs that fail to recover fine anatomical detail. Convolutional neural networks such as SRCNN [9] and EDSR [10] improved upon these baselines for natural images. Three-dimensional convolutional networks have been proposed for brain MRI SR [6], [7], demonstrating that exploiting inter-slice context yields measurable gains of 1–3 dB PSNR.

Denoising diffusion models [1] have emerged as powerful generative frameworks for image synthesis and restoration. Saharia et al. [3] demonstrated with SR3 that conditioning a diffusion model on a low-resolution input achieves state-of-the-art perceptual quality for image SR. Karras et al. [18] later elucidated the design space of diffusion models, introducing a continuous-sigma formulation with improved conditioning that we adopt in this work.

Our contributions are as follows:

- 1) We adapt the EDM framework [18], leveraging the mature U-Net and continuous-sigma conditioning codebase of DIAMOND [20], to volumetric MRI super-resolution, implementing both a 3D and a 2.5D variant.
- 2) We achieve 37.75 dB PSNR on $2\times$ brain MRI SR with the 3D model after 20 epochs of training on 59 subjects from the NKI cohort of FOMO60K [19], improving

on off-the-shelf EDSR and Swin2SR baselines by more than 2 dB PSNR in our evaluation setup.

- 3) We provide a systematic comparison of 3D volumetric versus 2.5D slice-conditioned diffusion approaches, analyzing the accuracy–compute trade-off.

II. RELATED WORK

A. CNN-Based MRI Super-Resolution

SRCNN [9] was among the first to apply deep learning to SR. EDSR [10] improved upon it with residual scaling. Chen et al. [6] proposed a 3D densely connected SR network (mDCSRN) for brain MRI, and Pham et al. [7] extended this to multi-scale architectures.

B. Diffusion-Based Super-Resolution

SR3 [3] conditions a DDPM on the LR input via channel concatenation. Xia et al. [12] enable partial diffusion for faster inference. Wu et al. [13] integrate residual shifting for sub-second MRI slice reconstruction.

C. Elucidated Diffusion Models

Karras et al. [18] reformulated diffusion models using a continuous noise level σ instead of discrete timesteps, with preconditioning functions c_{in} , c_{out} , c_{skip} , and c_{noise} that stabilize training and improve sample quality. This formulation was adopted by DIAMOND [20] for real-time world modeling in Atari games, which we repurpose for MRI super-resolution.

III. METHODS

A. Problem Formulation

Let $\mathbf{x}_{\text{HR}} \in \mathbb{R}^{D \times H \times W}$ denote a high-resolution MRI volume and $\mathbf{x}_{\text{LR}} \in \mathbb{R}^{D \times H' \times W'}$ its low-resolution counterpart ($H' = H/s$, $W' = W/s$ for scale factor s ; the depth dimension D is preserved, i.e., downsampling is applied in-plane only). The SR task seeks a mapping $f_{\theta} : \mathbf{x}_{\text{LR}} \mapsto \hat{\mathbf{x}}_{\text{HR}}$.

B. EDM Noise Conditioning

Following Karras et al. [18], we parameterize the diffusion process using a continuous noise level σ . The noisy observation is:

$$\mathbf{x}_{\sigma} = \mathbf{x}_{\text{HR}} + \sigma \cdot \epsilon, \quad \epsilon \sim \mathcal{N}(\mathbf{0}, \mathbf{I}). \quad (1)$$

Hendrik Chiche, Ludovic Corcos, and Logan Rouge are in collaboration with GENCI (Grand Équipement National de Calcul Intensif), France (e-mail: hendrik_chiche@berkeley.edu; ludovic.corcos@etu.uca.fr; logan.rouge@etu.uca.fr). This work was supported in part by GENCI for access to high-performance computing resources.

The denoiser D_θ is preconditioned as:

$$D_\theta(\mathbf{x}_\sigma, \sigma) = c_{\text{skip}} \mathbf{x}_\sigma + c_{\text{out}} F_\theta(c_{\text{in}} \mathbf{x}_\sigma, c_{\text{noise}}, \mathbf{x}_{\text{LR}}), \quad (2)$$

where F_θ is the U-Net backbone and the scaling functions are:

$$c_{\text{in}}(\sigma) = 1/\sqrt{\sigma^2 + \sigma_{\text{data}}^2}, \quad (3)$$

$$c_{\text{skip}}(\sigma) = \sigma_{\text{data}}^2/(\sigma^2 + \sigma_{\text{data}}^2), \quad (4)$$

$$c_{\text{out}}(\sigma) = \sigma \cdot \sqrt{c_{\text{skip}}(\sigma)}, \quad (5)$$

$$c_{\text{noise}}(\sigma) = \frac{1}{4} \ln \sigma. \quad (6)$$

During training, σ is sampled from a log-normal distribution: $\ln \sigma \sim \mathcal{N}(P_{\text{mean}}, P_{\text{std}}^2)$ with $P_{\text{mean}} = -1.2$, $P_{\text{std}} = 1.2$. The training loss is:

$$\mathcal{L} = \mathbb{E}_{\sigma, \mathbf{x}_{\text{HR}}, \epsilon} [\|D_\theta(\mathbf{x}_\sigma, \sigma) - \mathbf{x}_{\text{HR}}\|^2]. \quad (7)$$

C. Architecture A: 3D Convolutional U-Net

The 3D U-Net operates on volumetric tensors of shape (B, C, D, H, W) . The encoder has four levels with channel dimensions [32, 64, 128, 256], each containing 2 residual blocks with 3D convolutions ($3 \times 3 \times 3$), adaptive group normalization conditioned on c_{noise} , and SiLU activations. Multi-head self-attention with flash attention (`scaled_dot_product_attention`) is applied at the deepest level. The decoder mirrors the encoder with skip connections. Noise conditioning uses Fourier feature embeddings projected through an MLP. Total parameters: **50.7 M**.

The LR volume is trilinearly upsampled to the target resolution and concatenated with the noisy HR target along the channel dimension (2 input channels total).

During training, random 3D patches of size 32^3 (LR) and $32 \times 64 \times 64$ (HR, $2 \times$ in H/W) are extracted. Inference uses sliding-window patch processing with overlap blending and a 20-step Euler sampler; the choice of step count balances reconstruction quality against runtime (see Section VI).

D. Architecture B: 2.5D Slice-Conditioned U-Net

The 2.5D model decomposes the volumetric SR problem into per-slice 2D SR tasks with inter-slice conditioning. For each target slice at index i , the model receives: (1) one adjacent LR slice (bicubic-upsampled to HR resolution), (2) the target LR slice (also upsampled), and (3) the noisy HR target, concatenated along channels (3 channels total input). The 2D U-Net has channel dimensions [64, 64, 128, 256] with 2 residual blocks per level, self-attention at the deepest level, and the same EDM noise conditioning. A Heun solver with one denoising step (order-2 ODE solver) is used at inference. Total parameters: **51.1 M**.

E. Training Configuration

Both models are trained with AdamW ($\text{lr} = 10^{-4}$, weight decay = 10^{-2}). The 2.5D model is trained for 10 epochs with batch size 4, 8 gradient accumulation steps (effective batch 32), and 400 optimizer updates per epoch. The 3D model uses batch size 2 with 4 gradient accumulation steps, 8 patches per volume, and is reported after 20 epochs. Training is performed on a single NVIDIA L4 GPU (22 GB).

Algorithm 1 summarizes the EDM training procedure.

Algorithm 1 EDM-based MRI Super-Resolution Training

- 1: **repeat**
 - 2: Sample $(\mathbf{x}_{\text{LR}}, \mathbf{x}_{\text{HR}})$ from dataset
 - 3: Sample $\ln \sigma \sim \mathcal{N}(P_{\text{mean}}, P_{\text{std}}^2)$
 - 4: $\epsilon \sim \mathcal{N}(\mathbf{0}, \mathbf{I})$
 - 5: $\mathbf{x}_\sigma \leftarrow \mathbf{x}_{\text{HR}} + \sigma \cdot \epsilon$
 - 6: Compute $D_\theta(\mathbf{x}_\sigma, \sigma, \mathbf{x}_{\text{LR}})$ via (2)
 - 7: $\mathcal{L} \leftarrow \|D_\theta - \mathbf{x}_{\text{HR}}\|^2$
 - 8: Update θ via AdamW
 - 9: **until** convergence
-

IV. DATASET

We use the NKI (Nathan Kline Institute) cohort from the FOMO60K dataset [19], which provides T1-weighted structural brain MRI volumes from over 1,300 subjects. Each volume is acquired at approximately 1 mm isotropic resolution and stored in NIfTI format.

Ethics and consent: The study uses de-identified human brain MRI data from the publicly available FOMO60K/NKI dataset. Informed consent was obtained by the original data collection study, and the present work involves only secondary analysis of anonymized data.

Preprocessing: Volumes are intensity-normalized to $[0, 255]$ using the 1st–99th percentile range, then sliced along the sagittal axis. Each 2D slice is downsampled by a factor of 2 using block averaging to produce the LR input (128×128 pixels). The corresponding HR slice (256×256) serves as the ground truth. For 3D training, LR/HR volume pairs are stored directly, and random 3D patches are extracted during training. All tensors are normalized to $[-1, 1]$.

Train/test split: We process 59 subjects (100 scanning sessions) for training and hold out 5 subjects (6 sessions, 993 slices) for testing. The split is performed at the subject level to prevent data leakage—no subject appears in both sets.

V. RESULTS

A. Quantitative Metrics

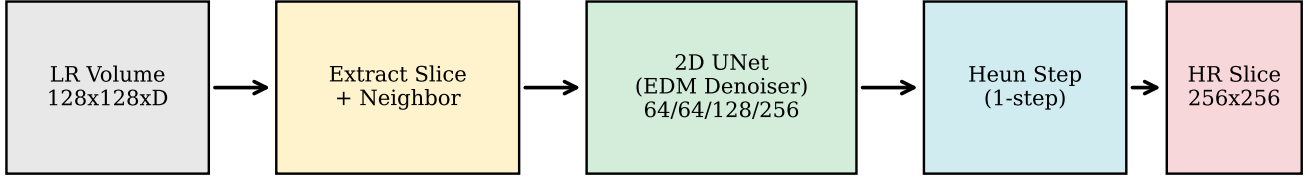
We report three standard full-reference image quality metrics: PSNR (Peak Signal-to-Noise Ratio), which measures pixel-level fidelity on the $[-1, 1]$ range (higher is better); SSIM (Structural Similarity Index) [17], which captures perceived structural quality (higher is better); and LPIPS (Learned Perceptual Image Patch Similarity) [21], which measures perceptual distance using AlexNet features (lower is better).

B. Main Results

Table I presents quantitative results on the NKI test set for $2 \times$ super-resolution.

The 3D EDM model (20 epochs) achieves **37.75 dB PSNR**, **0.997 SSIM**, and **0.020 LPIPS**, surpassing the best pretrained baseline (EDSR, 35.57 dB) by +2.18 dB in PSNR and also outperforming it in perceptual quality (LPIPS 0.020 vs. 0.024). The 3D EDM model thus achieves the best scores across *all three metrics* among the methods evaluated here. Because EDSR and Swin2SR use off-the-shelf DIV2K weights rather

(a) 2.5D Slice-Conditioned EDM Pipeline



(b) 3D Volumetric EDM Pipeline

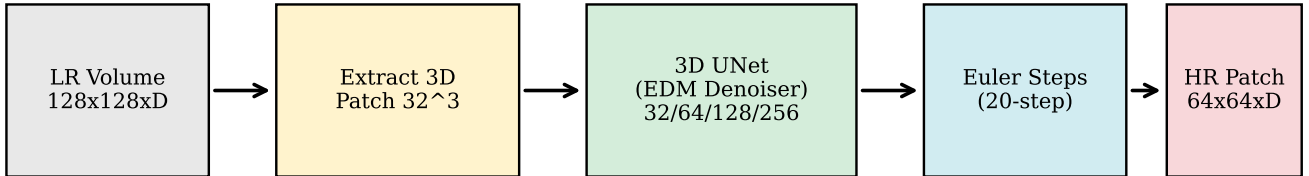


Fig. 1. Overview of the two super-resolution pipelines. (a) The 3D model (best-performing) extracts volumetric patches, processes them through a 3D U-Net with 20-step Euler sampling, and blends overlapping patches to reconstruct the full HR volume. (b) The 2.5D model extracts individual slices with one neighboring slice as context, processes each through a 2D U-Net with one-step Heun sampling, and stacks results.

TABLE I
QUANTITATIVE RESULTS FOR $2\times$ MRI SUPER-RESOLUTION ON THE NKI TEST SET (5 SUBJECTS, 993 SAGITTAL SLICES / 6 VOLUMES). ALL METHODS EVALUATED ON IDENTICAL TEST DATA AND DEGRADATION PIPELINE. EDSR AND SWIN2SR USE PRETRAINED DIV2K WEIGHTS WITHOUT MRI FINE-TUNING.

Method	PSNR \uparrow	SSIM \uparrow	LPIPS \downarrow	Params
Bicubic interpolation	33.89	0.957	0.091	—
EDSR [10] (DIV2K)	35.57	0.977	0.024	1.4M
Swin2SR [22] (DIV2K)	35.50	0.978	0.024	1.0M
2.5D EDM (ours, 10 ep)	35.82	0.971	0.040	51.1M
3D EDM (ours, 20 ep)	37.75	0.997	0.020	50.7M

than MRI-specific training, this comparison should be interpreted as a strong reference point rather than a fully matched training comparison. The 2.5D EDM model also outperforms EDSR by +0.25 dB PSNR while improving over bicubic interpolation by +1.93 dB. Fig. 2 visualizes these comparisons.

C. Comparison with Pretrained Baselines

To enable a rigorous apples-to-apples comparison, we evaluate two state-of-the-art pretrained SR models—EDSR [10] and Swin2SR [22]—on the *exact same* test set using the *identical degradation pipeline*. Both baselines use DIV2K-pretrained weights without any MRI fine-tuning; grayscale slices are converted to 3-channel input via channel replication. Results are reported in Table I. Fig. 3 shows a visual comparison on a

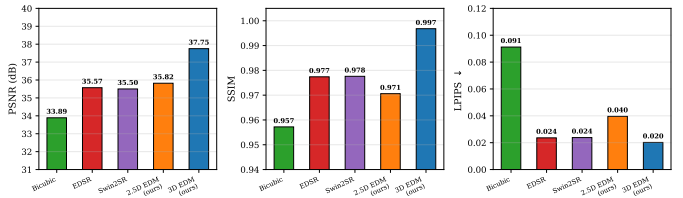


Fig. 2. PSNR and SSIM comparison across methods for $2\times$ MRI SR on the NKI test set. The 3D EDM model achieves the strongest PSNR and SSIM among the evaluated methods.

mid-sagittal slice with a zoomed region of interest highlighting cortical detail recovery.

D. Per-Subject Analysis

Table II presents a per-subject breakdown for the 3D EDM, 2.5D EDM, and bicubic methods on five test volumes. The 3D model consistently achieves the highest PSNR and SSIM and the lowest LPIPS across all subjects.

E. Per-Slice Reconstruction Quality

Fig. 4 shows the per-slice PSNR across the sagittal axis for one test subject. The 2.5D model maintains relatively uniform quality, with higher PSNR near the volume edges where slices contain less complex anatomy and are easier to reconstruct.

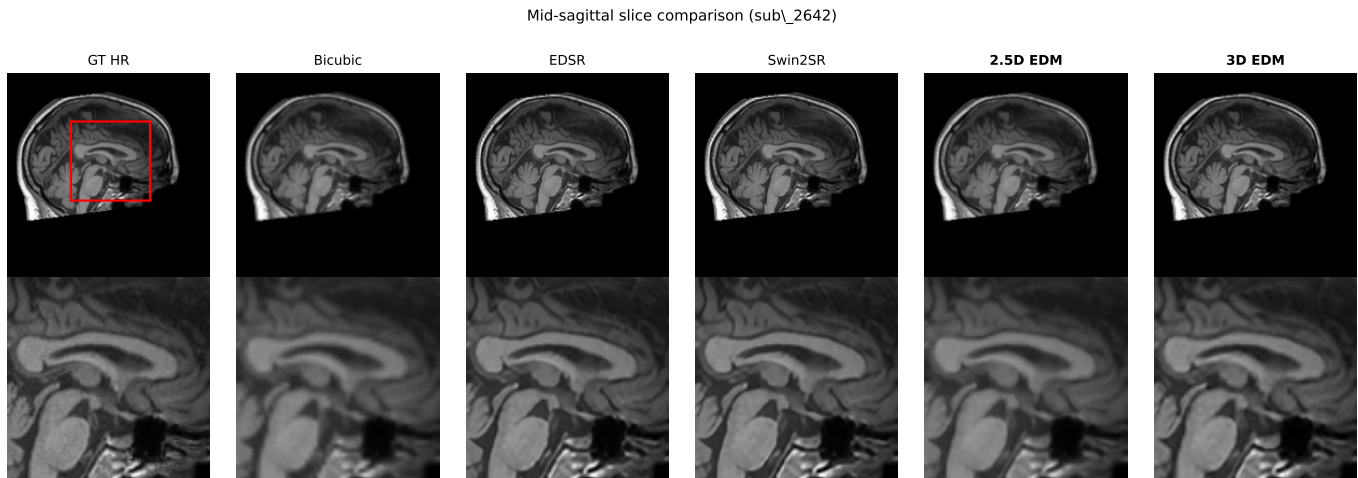


Fig. 3. Visual comparison of all methods on a mid-sagittal slice (sub_2642). Top row: full slice. Bottom row: zoomed region of interest (red box) showing cortical folds and gray/white matter boundaries. The 3D EDM model recovers the sharpest anatomical detail, while EDSR and Swin2SR produce smoother outputs. Bicubic interpolation exhibits visible blurring.

TABLE II

PER-SUBJECT EVALUATION ON THE NKI TEST SET (5 VOLUMES). ALL METHODS EVALUATED ON IDENTICAL TEST DATA AND DEGRADATION PIPELINE.

Subject	3D EDM (ours)			2.5D EDM (ours)			Bicubic		
	PSNR	SSIM	LPIPS	PSNR	SSIM	LPIPS	PSNR	SSIM	LPIPS
sub_2642	37.44	0.996	0.022	35.52	0.968	0.043	33.59	0.954	0.097
sub_2952	38.15	0.997	0.019	36.79	0.971	0.038	35.34	0.956	0.089
sub_6794 (ses1)	37.33	0.997	0.020	34.64	0.971	0.040	32.19	0.958	0.095
sub_6794 (ses2)	37.74	0.997	0.020	35.41	0.972	0.041	33.32	0.959	0.093
sub_8390	38.10	0.996	0.020	35.97	0.970	0.038	33.87	0.956	0.090
Average	37.75	0.997	0.020	35.67	0.970	0.040	33.66	0.957	0.093

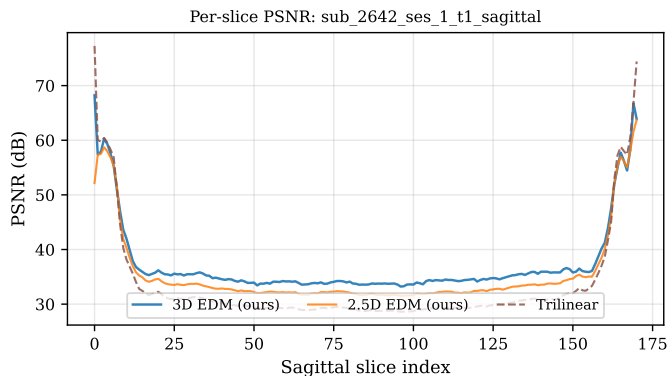


Fig. 4. Per-slice PSNR across the sagittal axis for subject sub_2642 (2.5D model).

F. Visual Comparison

We select the 3D model for visual comparison because it enables inspection across all three orthogonal planes from a single volumetric reconstruction. Fig. 5 shows that the model produces sharper cortical boundaries and clearer gray/white matter contrast compared to trilinear interpolation.

G. Per-Pixel Error Analysis

Fig. 6 shows the per-pixel absolute error for a mid-sagittal slice, comparing bicubic, trilinear, and EDM reconstructions against the ground truth. Both EDM models produce lower error in cortical regions and at tissue boundaries compared to the interpolation baselines, with the 3D model achieving the lowest error overall. The highest residual errors for all methods concentrate at the skull boundary and air-tissue interfaces.

VI. DISCUSSION

A. 3D vs. 2.5D Performance Gap

The 3D model (20 epochs) outperforms the 2.5D variant by +1.93 dB PSNR, +0.026 SSIM, and halves the LPIPS (0.020 vs. 0.040). This gap reflects the advantage of native volumetric processing: 3D convolutions capture inter-slice anatomical continuity that the 2.5D model, conditioned on only one neighboring slice, cannot fully exploit. The 3D model also surpasses the best pretrained baseline (EDSR, 35.57 dB / 0.024 LPIPS) by +2.18 dB PSNR *and* achieves better perceptual quality (LPIPS 0.020). Given that the CNN baselines were not fine-tuned on MRI data, we interpret this result as evidence that MRI-specific diffusion training is highly competitive and effective under the present evaluation setup.

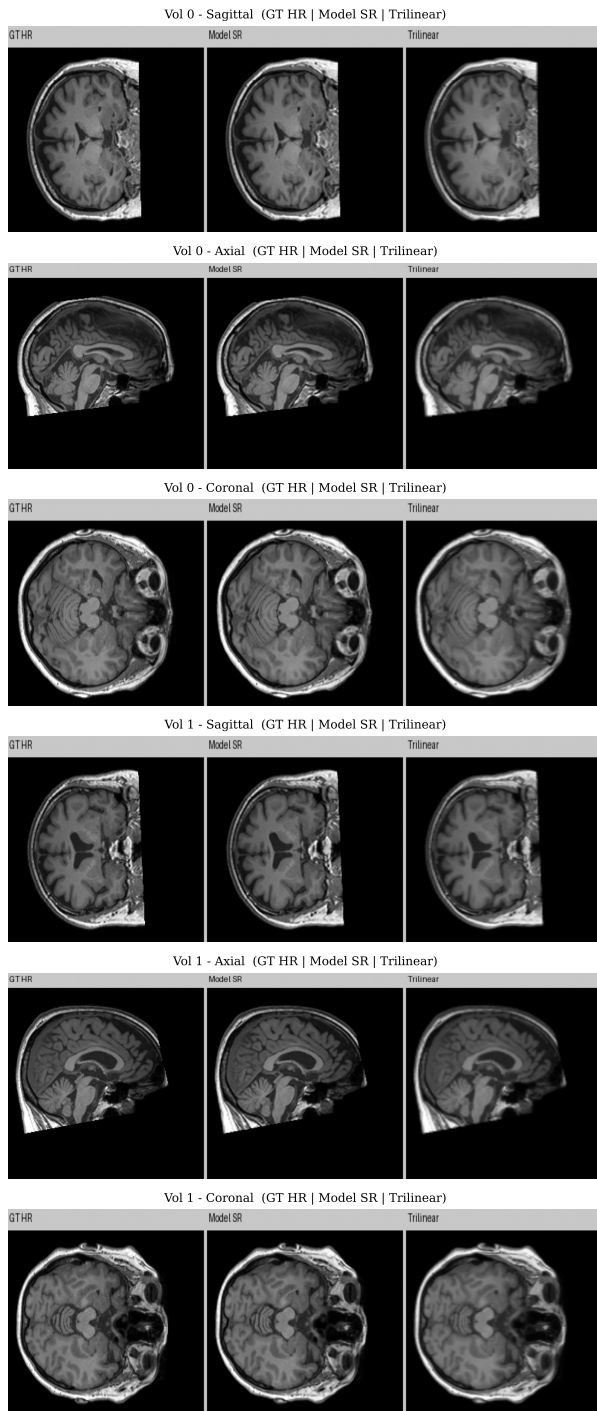


Fig. 5. 3D EDM model visual comparison across sagittal, axial, and coronal views. Each panel shows (left to right): ground truth HR, 3D model prediction, and trilinear baseline. The 3D model recovers fine cortical detail and interslice continuity lost in interpolation.

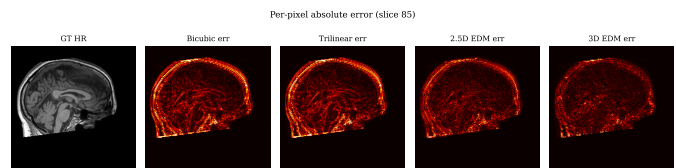


Fig. 6. Per-pixel absolute error heatmaps for a mid-sagittal slice. Darker regions indicate lower reconstruction error. The EDM models show reduced error in cortical folds and gray/white matter boundaries compared to bicubic and trilinear interpolation; the 3D model achieves the lowest overall error (see Table I).

B. EDM Framework Advantages

Our adoption of the EDM formulation [18] rather than the original DDPM [1] offers several practical benefits: (i) the continuous-sigma parameterization simplifies the noise schedule design, (ii) the preconditioning functions stabilize training, and (iii) the framework naturally supports variable numbers of sampling steps—enabling one-step Heun inference for the 2.5D model and 20-step Euler inference for the 3D model.

C. Inference Efficiency

The 2.5D model with one-step Heun sampling achieves 0.09s per slice on Apple MPS, enabling near-real-time processing of full volumes (~ 15 s for 170 slices). The 3D model requires patch-based inference with overlap blending, taking approximately 10 minutes per volume on MPS—suitable for offline processing but not real-time applications.

D. Flash Attention

We replace the standard quadratic self-attention with PyTorch’s `scaled_dot_product_attention`, which dispatches to flash attention on CUDA GPUs when a compatible kernel is available. In practice, this avoids materializing the full attention matrix, substantially reducing attention-memory overhead and improving training throughput, which enables batch size 4 training on 22 GB L4 GPUs where the original implementation would require batch size 2.

E. Limitations

Our evaluation is conducted on a single dataset (NKI/FOMO60K) with image-domain downsampling. Clinical MRI degradation involves k-space truncation, noise, and motion artifacts that are not modeled here. While the 2.5D model achieves a higher LPIPS (0.040) than EDSR/Swin2SR (0.024), the 3D model with extended training (20 epochs) surpasses them across all metrics including LPIPS (0.020), indicating that with sufficient volumetric training, diffusion models can be highly competitive in perceptual quality on this task. Additionally, only 5 test subjects are used due to dataset access constraints; larger-scale evaluation would strengthen conclusions.

An important caveat regarding the baseline comparison is that our EDM models were trained on NKI brain MRI data, whereas the EDSR and Swin2SR baselines use pretrained weights from DIV2K—a natural-image dataset that contains

no medical imagery. This domain mismatch inherently disadvantages these baselines; retraining EDSR or Swin2SR on MRI data would likely improve their performance substantially. A fully fair comparison would require training all methods on the same MRI training set, which we leave to future work. Nevertheless, the apples-to-apples evaluation on identical test data and degradation establishes a useful reference point and shows that domain-specific training offers a clear advantage over the off-the-shelf natural-image SR models considered here.

VII. CONCLUSION

We presented a comparative study of two U-Net architectures for EDM-based MRI super-resolution: a native 3D convolutional U-Net and a 2.5D slice-conditioned approach, both building on the EDM codebase provided by the DIAMOND framework [20]. The 3D model achieves 37.75 dB PSNR, 0.997 SSIM, and 0.020 LPIPS on the NKI test set, outperforming the off-the-shelf pretrained EDSR and Swin2SR baselines used in our evaluation across all three metrics, while requiring only 20 epochs of training on 59 subjects. The 2.5D model offers a lightweight alternative with near-real-time one-step inference (35.82 dB PSNR) at the cost of reduced volumetric consistency.

Future directions include: (1) scaling to the full FOMO60K dataset (~60,000 subjects) and evaluating on standard benchmarks (HCP, IXI); (2) training the 2.5D model on all three anatomical axes and ensembling predictions; (3) clinical validation with expert radiologist assessment; (4) modeling realistic k-space degradation; and (5) enabling multi-stage training with learning rate scheduling.

ACKNOWLEDGMENT

This work was supported in part by GENCI (Grand Équipement National de Calcul Intensif) for access to high-performance computing resources.

REFERENCES

- [1] J. Ho, A. Jain, and P. Abbeel, “Denoising diffusion probabilistic models,” in *Advances in Neural Information Processing Systems*, vol. 33, pp. 6840–6851, 2020.
- [2] A. Q. Nichol and P. Dhariwal, “Improved denoising diffusion probabilistic models,” in *Proc. 38th Int. Conf. Machine Learning (ICML)*, pp. 8162–8171, 2021.
- [3] C. Saharia *et al.*, “Image super-resolution via iterative refinement,” *IEEE Trans. Pattern Anal. Mach. Intell.*, vol. 45, no. 4, pp. 4713–4726, 2022.
- [4] O. Ronneberger, P. Fischer, and T. Brox, “U-Net: Convolutional networks for biomedical image segmentation,” in *Medical Image Computing and Computer-Assisted Intervention – MICCAI 2015*, pp. 234–241, 2015.
- [5] Ö. Çiçek *et al.*, “3D U-Net: Learning dense volumetric segmentation from sparse annotation,” in *MICCAI 2016*, pp. 424–432, 2016.
- [6] Y. Chen *et al.*, “Brain MRI super resolution using 3D deep densely connected neural networks,” in *2018 IEEE 15th Int. Symp. Biomedical Imaging (ISBI)*, pp. 739–742, 2018.
- [7] C.-H. Pham, A. Ducournau, R. Fablet, and F. Rousseau, “Multiscale brain MRI super-resolution using deep 3D convolutional networks,” *Comput. Med. Imaging Graph.*, vol. 77, p. 101647, 2019.
- [8] D. C. Van Essen *et al.*, “The WU-Minn Human Connectome Project: An overview,” *NeuroImage*, vol. 80, pp. 62–79, 2013.
- [9] C. Dong, C. C. Loy, K. He, and X. Tang, “Image super-resolution using deep convolutional networks,” *IEEE Trans. Pattern Anal. Mach. Intell.*, vol. 38, no. 2, pp. 295–307, 2016.

- [10] B. Lim, S. Son, H. Kim, S. Nah, and K. M. Lee, “Enhanced deep residual networks for single image super-resolution,” in *Proc. IEEE Conf. Comput. Vis. Pattern Recognit. Workshops*, pp. 136–144, 2017.
- [11] J. Ouyang, Y. Zhang, S. Chen, G. Li, and Z. Wang, “Advancing 1.5T MR imaging: Toward achieving 3T quality through deep learning super-resolution techniques,” *Frontiers in Human Neuroscience*, vol. 19, p. 1532395, 2025.
- [12] K. Xia, M. Soltanolkotabi, R. M. Leahy, and J. E. Iglesias, “MRI super-resolution with partial diffusion models,” *IEEE Trans. Med. Imaging*, vol. 43, no. 5, pp. 1660–1672, 2024.
- [13] M. Wu, H. Li, J. Zhang, and S. K. Zhou, “MRI super-resolution reconstruction using efficient diffusion probabilistic model with residual shifting,” *arXiv preprint arXiv:2503.01576*, 2025.
- [14] Y. Song and S. Ermon, “Generative modeling by estimating gradients of the data distribution,” in *Advances in Neural Information Processing Systems*, vol. 32, pp. 11918–11930, 2019.
- [15] P. Dhariwal and A. Nichol, “Diffusion models beat GANs on image synthesis,” in *Advances in Neural Information Processing Systems*, vol. 34, pp. 8780–8794, 2021.
- [16] A. Vaswani *et al.*, “Attention is all you need,” in *Advances in Neural Information Processing Systems*, vol. 30, pp. 5998–6008, 2017.
- [17] Z. Wang, A. C. Bovik, H. R. Sheikh, and E. P. Simoncelli, “Image quality assessment: From error visibility to structural similarity,” *IEEE Trans. Image Processing*, vol. 13, no. 4, pp. 600–612, 2004.
- [18] T. Karras, M. Aittala, T. Aila, and S. Laine, “Elucidating the design space of diffusion-based generative models,” in *Advances in Neural Information Processing Systems*, vol. 35, pp. 26565–26577, 2022.
- [19] FOMO-MRI Consortium, “FOMO60K: A large-scale multi-site MRI dataset for brain imaging research,” Zenodo / HuggingFace Datasets, 2024. [Online]. Available: <https://huggingface.co/datasets/FOMO-MRI/FOMO60K>
- [20] E. Alonso *et al.*, “DIAMOND: Diffusion for world modeling: Visual details matter in Atari,” in *Advances in Neural Information Processing Systems*, vol. 37, 2024.
- [21] R. Zhang, P. Isola, A. A. Efros, E. Shechtman, and O. Wang, “The unreasonable effectiveness of deep features as a perceptual metric,” in *Proc. IEEE Conf. Comput. Vis. Pattern Recognit. (CVPR)*, 2018, pp. 586–595.
- [22] M. V. Conde, U.-J. Choi, M. Burber, and R. Timofte, “Swin2SR: SwinV2 Transformer for compressed image super-resolution and restoration,” in *European Conf. Comput. Vis. Workshops (ECCVW)*, 2022, pp. 669–687.